TRIB3 Promotes Osteogenic Differentiation of Human Adipose-derived Mesenchymal Stem Cells Levelled by Post-transcriptional Regulation of miR-24-3p

Xiang Song BAI[1], Ping ZHANG[1], Yun Song LIU[1], Hao LIU[2], Long Wei LV[1], Yong Sheng ZHOU[1]

Objective: *To explore the effect of TRIB3 on the osteogenic differentiation of human adipose-derived mesenchymal stem cells (hASCs) and reveal the potential role of TRIB3 in bone regeneration.*

Methods: *TRIB3-knockdown and TRIB3-overexpression hASCs were used to explore the effect of TRIB3 on osteogenic differentiation by alkaline phosphatase (ALP) staining, alizarin red S (ARS) staining, quantitative real-time polymerase chain reaction (qRT-PCR) and heterotopic bone formation. The regulation of miR-24-3p on TRIB3 was detected by qRT-PCR and western blot. Ribonucleic acid (RNA) sequencing was performed to investigate the downstream regulatory network of TRIB3.*

Results: *TRIB3 promoted the osteogenic differentiation of hASCs both in vitro and in vivo. This process was regulated epigenetically by the post-transcriptional regulation of miR-24-3p, which could bind directly to the three prime untranslated region (3'UTR) of TRIB3 and inhibit TRIB3 expression. The downstream regulatory network of TRIB3-mediated osteogenic differentiation was related to calcium ion binding and cell metabolism, extracellular signal-regulated protein kinases 1 and 2 (ERK1/2) and nuclear factor-κB (NF-κB) signalling pathways.*

Conclusion: *TRIB3 is a promising therapeutic target for hASC-based bone tissue engineering and the epigenetic regulation of TRIB3 through miR-24-3p permits regulatory controllability, thus promoting osteogenesis through an important metabolic target while obtaining a safe and controllable effect via post-transcriptional epigenetic regulation.*

Key words: *epigenetic regulation, human adipose-derived mesenchymal stem cells, miR-24-3p, osteogenic differentiation, TRIB3*

Chin J Dent Res 2021;24(4):235–249; doi: 10.3290/j.cjdr.b2440815

1 Department of Prosthodontics, Peking University School and Hospital of Stomatology & National Centre of Stomatology & National Clinical Research Centre for Oral Disease & National Engineering Laboratory for Digital and Material Technology of Stomatology & Beijing Key Laboratory of Digital Stomatology, Key Laboratory of Digital Stomatology & Research Centre of Engineering and Technology for Computerized Dentistry Ministry of Health & NMPA Key Laboratory for Dental Materials, Beijing, P.R. China.

2 The Central Laboratory, Peking University School and Hospital of Stomatology, Beijing, P.R. China.

Corresponding author: Dr Long Wei LV, Department of Prosthodontics, Peking University School and Hospital of Stomatology, #22 Zhongguancun South Avenue, Haidian District, Beijing, 100081, P.R. China. Tel: 86-10-82195393; Fax: 86-10-62173402.Email: lvlw@bjmu.edu.cn

This study was supported by a grant from the Beijing Natural Science Foundation (7192228), National Natural Science Foundation of China (31600787) and the Young Elite Scientist Sponsorship Programme by CAST (2015QNRC001).

Bone tissue engineering has been considered a promising method for the treatment of oral and maxillofacial bone defects, and human adipose-derived mesenchymal stem cells (hASCs) have been regarded as one of the most promising seed cells in the clinical transformation of bone tissue engineering due to their easy accessibility, abundance, lower donor site morbidity and multilineage differentiation capability[1,2]; however, promoting the osteogenic differentiation of hASCs efficiently while protecting these candidate seed cells from overdifferentiation remains a problem[3,4]. Thus, further exploration of the key influencing factors of the osteogenic differentiation and balancing regulatory networks is paramount to the clinical transformation of bone tissue engineering, a promising therapeutic method for bone defects that have been considered a common clinical problem and placed a considerable burden on patients as well as the health care system[4,5].

Pseudokinases, lacking one or more of the conserved amino acids in the kinase domain, are a group of pseudoenzymes that are unable to phosphorylate protein substrates, but still perform pivotal nonenzymatic roles in regulating diverse physiological and pathological processes[6]. The tribbles pseudokinases (TRIB) represent a subbranch of the CAMK subfamily and contain three domains including an N-terminal PEST region, a pseudokinase domain and a C-terminal COP-1 binding peptide region[7]. The three related TRIB family members (TRIB1-3) are classified as serine/threonine pseudokinases that either lack (TRIB1) or have low (TRIB2 and TRIB3) vestigial ATP affinity and phosphotransferase capacity. Among these, tribbles pseudokinase 3 (TRIB3) governs multiple aspects of important metabolic and biological processes[8] including insulin resistance[9-13], lipid metabolism[14] and autophagy[15], which renders TRIB3 a promising therapeutic target for metabolic and ageing-related diseases such as type II diabetes[10], hyperlipidemia[16], atherosclerosis[17] and Alzheimer's disease[18]. Although bone metabolism and regeneration are closely related to the general metabolic state[19], little is known about the function and regulatory mechanisms of TRIB3, a key factor in metabolic regulation, in the osteogenesis of hASCs.

Micro ribonucleic acids (microRNAs), noncoding single-stranded RNAs composed of approximately 20 to 24 nucleotides, have been recognised to form the complex post-transcriptional regulatory networks in epigenetic regulation[20]. MicroRNAs negatively regulate gene expression by binding with the three prime untranslated region (3' UTR) of target messenger RNAs in a partial or fully complementary manner, and play key roles in the maintenance and lineage commitment of mesenchymal stem cells[21,22]. The microRNA regulatory network is crucial in bone homeostasis[23-25] and helps to protect targeted genes from overexpression by post-transcriptional regulation, an epigenetic regulatory pattern that does not alter the DNA sequences[26]. Meanwhile, microRNAs are endogenous biomolecules in eukaryotes and their expressions and regulating patterns vary in different tissues or cells[27]; however, as an important metabolic target, the post-transcriptional regulation of TRIB3 by microRNAs, especially in hASCs, has not been reported.

Thus, the present study explored the novel role of TRIB3 in the osteogenic differentiation of hASCs and confirmed that miR-24-3p was a negative regulator that protected hASCs from overdifferentiation by targeting TRIB3 through post-transcriptional regulation. Moreover, RNA sequencing and bioinformatic analyses revealed the downstream regulatory networks of TRIB3-mediated osteogenic differentiation of hASCs, in which calcium ion binding and cell metabolism, extracellular signal-related protein kinases 1 and 2 (ERK1/2) and nuclear factor-κB (NF-κB) signalling pathways played important roles after TRIB3 overexpression. As such, TRIB3 is a promising therapeutic target for hASC-based bone tissue engineering and the epigenetic regulation of TRIB3 through miR-24-3p permits regulatory controllability, thus promoting osteogenesis through an important metabolic target while obtaining a safe and controllable effect via post-transcriptional regulation.

Materials and methods

Cell culture

hASCs were purchased from ScienCell (San Diego, CA, USA), and cultured in proliferation medium (PM) comprised of Dulbecco's modified Eagle medium (DMEM; Gibco, Grand Island, NY, USA), 10% (v/v) foetal bovine serum (FBS; ScienCell), 100 U/ml penicillin G and 100 mg/ml streptomycin (Gibco) at 37°C in an incubator with 5% CO_2 atmosphere and 100% relative humidity. Cells at the fourth passage were used for the experiments. The osteogenic medium (OM) consisted of fresh DMEM containing 10% (v/v) FBS, 100 U/ml penicillin G and 100 mg/ml streptomycin, 10 nM dexamethasone (Sigma-Aldrich, St. Louis, MO, USA), 10 mM β-glycerophosphate (Sigma-Aldrich) and 50 μg/ml L-ascorbic acid (Sigma-Aldrich)[28]. All cell-based in vitro experiments were repeated three times.

Lentivirus transfection

Lentivirus transfection was performed as described previously[29]. All recombinant lentiviruses were purchased from GenePharma (Shanghai, China) and used for hASC transfection at a multiplicity of infection (MOI) of 100. The packaged lentiviruses used were antisense TRIB3 (shTRIB3#1 & shTRIB3#2), antisense negative control (sh-NC), TRIB3 overexpression (TRIB3-over), NC overexpression (NC-over), pre-miR-24-3p (miR-24-3p mimics) and antisense miR-24-3p (anti-miR-24-3p). The sequences are listed in Table S1 (not published, provided on request). hASCs were transfected in the fresh medium containing the dilutions of the viral supernatant and polybrene (5 μg/ml) for 24 hours, followed by selection with puromycin (Sigma-Aldrich) at 1 μg/ml. After 3 days of selection by puromycin, transduction efficiency was evaluated by the percentage of green fluorescent

Table 1 Primers for qRT-PCR.

Gene	Forward primers (5' to 3')	Reverse primers (5' to 3')
GAPDH	CGGACCAATACGACCAAATCCG	AGCCACATCGCTCAGACACC
TRIB3	GGGTCTGTTTTGCATGCGAGC	AGCTCGTTTCTGGACGGGAC
RUNX2	TCTTAGAACAAATTCTGCCCTTT	TGCTTTGGTCTTGAAATCACA
ALP	GACCTCCTCGGAAGACACTC	TGAAGGGCTTCTTGTCTGTG
OSX	CCTCCTCAGCTCACCTTCTC	GTTGGGAGCCCAAATAGAAA
OCN	AGCAAAGGTGCAGCCTTTGT	GCGCCTGGGTCTCTTCACT
VLDLR	CAGTGCCATATGAGAACATGCCG	AGTAGAATGGGCGCCACAGC
GRIN1	GCCTACAAGCGGCACAAGGA	TCAGTGGGATGGTACTGCTGC

ALP, alkaline phosphatase; GAPDH, glyceraldehyde-3-phosphate dehydrogenase; GRIN1, glutamate ionotropic receptor NMDA type subunit 1, OCN, osteocalcin; OSX, osterix, RUNX2, runt-related transcription factor 2; TRIB3, tribbles pseudokinase 3; VLDLR, very low density lipoprotein receptor.

protein (GFP)–positive cells observed under an inverted fluorescence microscope (TE2000-U, Nikon, Tokyo, Japan), as well as quantitative real-time polymerase chain reaction (qRT-PCR) for RNA expression analysis and western blot for protein analysis.

RNA extraction and qRT-PCR

hASCs were seeded in 6-well plates at a density of 2×10^5 cells per well. The total RNAs were extracted with TRIzol reagent (Invitrogen, Carlsbad, CA, USA) and reverse-transcribed into cDNA using the Reverse Transcription System (Takara, Tokyo, Japan). Briefly, 500 ng cellular RNAs were reverse transcribed to cDNAs according to the following settings: 37°C for 15 minutes, 85°C for 5 seconds and stored at 4°C. qRT-PCR was conducted using a 7500 Real-Time PCR Detection System (Applied Biosystems, Foster City, CA, USA) with a Power SYBR Green Master Mix (Roche, Basel, Swiss) according to the following settings: 95°C for 10 minutes, 40 cycles of 95°C for 15 seconds and 60°C for 1 minute on the ABI PRISM 7500 sequence detection system (Applied Biosystems). The internal controls for mRNAs were GAPDH. The primers (GAPDH, TRIB3, RUNX2, ALP, OSX, OCN, VLDLR and GRIN1) used for amplification were synthesised by Sangon Biotech (Shanghai, China) and are listed in Table 1.

As for miRNA, total RNAs of cells were extracted with TRIzol reagent and 1000 ng cellular RNAs were reverse-transcribed to cDNAs using Bulge-Loop miRNA qRT-PCR Starter Kit (RiboBio, Guangzhou, China) according to the following settings: 42°C for 60 minutes, 70°C for 10 minutes and stored at 4°C. The real-time PCR assay after stem-loop reverse transcription was performed under the following conditions: 95°C for 10 minutes, 40 cycles of 95°C for 2 seconds, 60°C for 20 seconds and 70°C for 10 seconds. The internal standard for miRNA was U6. The sequence of hsa-miR-24-3p was UGGCUCAGUUCAGCAGGAACAG. The miRNA qRT-PCR primer was synthesised by RiboBio. The cycle threshold values (Ct values) were used to calculate the fold differences using the 2-ΔΔCt relative expression method[30].

Western blot

Total protein extraction and western blot were performed as described previously[28]. Briefly, cells were harvested, washed with phosphate-buffered saline (PBS) and lysed in radioimmunoprecipitation assay (RIPA) buffer. Protein concentrations were determined by the BCA Protein Assay Kit (Thermo Pierce, Waltham, MA, USA). Proteins were separated by 10% sodium dodecyl sulphate polyacrylamide gel electrophoresis and transferred to poly(vinylidene fluoride) (PVDF) membranes. The primary antibodies, anti-TRIB3 (sc-271572, Santa Cruz Biotechnology, Dallas, TX, USA) and anti-GAPDH (5174, Cell Signaling Technology, Danvers, MA, USA), were diluted 1:1000 and incubated with the membranes at 4°C overnight, respectively. Horseradish peroxidase (HRP)-conjugated anti-mouse or anti-rabbit secondary antibodies (Cell Signaling Technology) were diluted 1:10,000 respectively and incubated with the membranes at room temperature for 1 hour. The immunoreactive protein bands were visualised using an ECL kit (CEBIO, Beijing, China). Band intensities were quantified using ImageJ software (https://imagej.nih.gov/ij/). The background was subtracted and the signal of each target band was normalised to that of the GAPDH band[31].

Alkaline phosphatase assays

hASCs were seeded in 6-well plates. Alkaline phosphatase (ALP) activity was detected after 7 and 14 days of osteoinduction. Cells were washed three times with PBS and fixed with 95% ethanol for 30 minutes. The

NBT/BCIP staining kit (CoWin Biotech, Beijing, China) was used for ALP staining[32].

Mineralisation assays

Mineralizsation was examined using alizarin red S (ARS) staining after 14 and 21 days of osteoinduction. Cells were washed three times with PBS and fixed with 95% ethanol for 30 minutes, then stained with 1% ARS staining solution (pH 4.2, Sigma-Aldrich) at room temperature. To quantify matrix calcification, ARS was dissolved with 100 mM cetylpyridinium chloride for 1 hour. Mineral accumulation was quantified by measuring the absorbance at 562 nm after completely dissolving the staining[32].

Heterotopic bone formation assay in vivo

The hASCs, stably infected with sh-NC, shTRIB3#1, shTRIB3#2, NC-over and TRIB3-over, were cultured in PM for 1 week. 1×10^6 cells from each group were trypsinised and resuspended respectively, and subsequently inoculated into cryotubes containing 40 mg beta-tricalcium phosphate (β-TCP; Bicon, Boston, MA, USA) particles at 37°C for 1 hour in a shaker, then centrifuged at 150 g for 5 minutes and implanted into the dorsal subcutaneous spaces of 6-week-old BALB/c homozygous nude (nu/nu) mice (six mice in each group; Vital River Laboratory Animal Technology, Beijing, China), as described previously[29]. This study was approved by the Institutional Animal Care and Use Committee of Peking University Health Science Centre (LA2014233). All the animal experiments were performed in accordance with the institutional animal guidelines. Specimens were harvested at 4 weeks and 8 weeks after surgery, fixed in 4% paraformaldehyde, decalcified in 10% ethylene diamine tetraacetic acid (EDTA, pH 7.4) for 14 days, then dehydrated and embedded in paraffin. Haematoxylin and eosin (H&E), Masson's trichrome and immunohistochemical staining with a primary antibody against osteocalcin (OCN; Abcam, ab13418) were used for slice staining. Tissue slices were visualised under a light microscope (Olympus, Tokyo, Japan). For quantification of osteoid tissue, two images of each sample (12 images per group) were taken randomly. ImageJ software was used to measure the percentage of new bone or collagen formation area [(bone or collagen area/total tissue area) * 100%], and mean density of OCN staining (integrated optical density of positive staining/cell containing tissue area) was measured for immunohistochemical staining[29,33].

Dual-luciferase reporter assay

Luciferase reporter assays were performed as described in a previous study by the present authors[34]. In brief, the TRIB3 cDNA fragments containing the predicted potential miR-24-3p-binding sites were amplified by PCR method and cloned to pEZX-MT06 vector (GeneCopoeia, Rockville, MD, USA) to form a wildtype TRIB3 (TRIB3-WT) luciferase reporter plasmid. The mutation of miR-24-3p target sites in the TRIB3 3'UTR was achieved by using a site-directed mutagenesis kit (SBS Genetech, Beijing, China) and a mutant type TRIB3 (TRIB3-MT) luciferase reporter plasmid was obtained.

293T cells were grown in a 24-well plate and cotransfected with 400 ng of either control plasmid or plasmid-expressing targeting gene, 40 ng firefly luciferase reporter plasmid and 4 ng pRL-TK, a plasmid-expressing Renilla luciferase (FulenGen, Guangzhou, China). Renilla and firefly luciferase activities were measured 24 hours after transfection using Dual-Luciferase Reporter Assay System (Promega, Madison, WI, USA). All luciferase values were normalised to those of Renilla luciferase and expressed as fold induction relative to the basal activity.

RNA sequencing and bioinformatic analyses

Total RNAs of TRIB3-over and NC-over hASCs cultured in PM or OM for 7 days were harvested. One microgram of RNA was used for cDNA library construction and mRNA sequencing by Beijing Genomics Institute using the BGISEQ-500 platform. High-quality reads were mapped to the human reference genome [GRCh38.p11(hg38)] using Bowtie 2. The levels of expression for each gene were normalised to fragments per kilobase of exon model per million mapped reads (FPKM) using RNA sequencing by Expectation Maximization (RSEM). The sequencing data were deposited in the Sequence Read Archive (SRA), and the access number for the sequencing data in the present study is PRJNA633723. Identification of differentially expressed genes (DEGs) was conducted with the Limma package in the R platform (R Core Team, Vienna, Austria). Differential gene expression presenting a log2 fold change ($\log2FC \geq |1|$, e.g., expression changes ≥ 2 or ≤ 0.5, and $Q < 0.05$ was identified as a DEG. The mean expression levels (standardised mean FPKM) of representative DEGs were illustrated in heatmap in the pheatmap package in R. DAVID Bioinformatics Resources 6.8 (https://david.ncifcrf.gov/, Laboratory of Immunopathogenesis and Bioinformatics) and the Ingenuity Pathways Analysis (IPA, Ingenuity Systems, Redwood City, CA, USA) platform (www.ingenuity.com) were used for

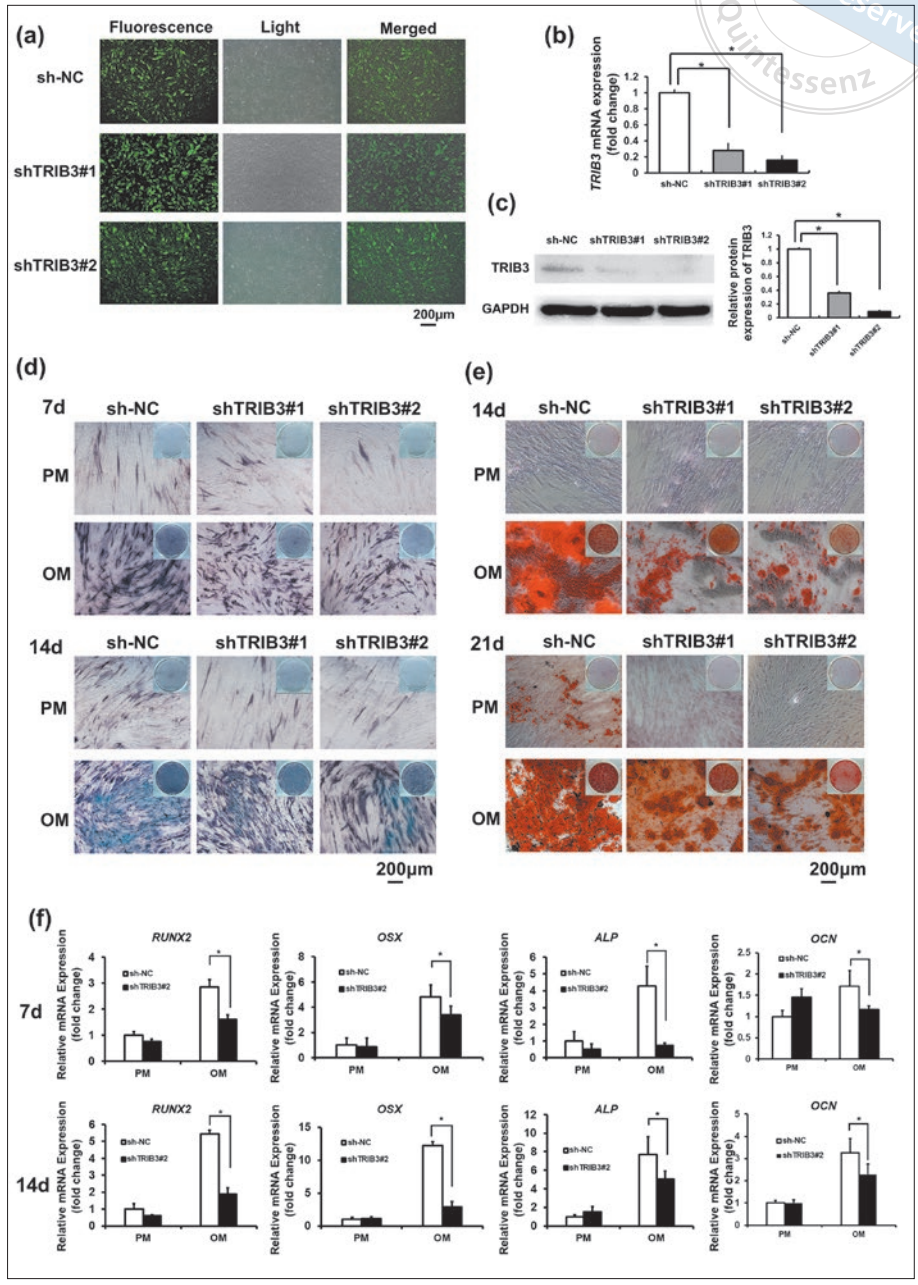

Fig 1 TRIB3 knockdown inhibited the osteogenic differentiation of hASCs in vitro**. (a)** Microscopic images of GFP-positive hASCs after lentivirus (sh-NC, shTRIB3#1 and shTRIB3#2) transfection under light and fluorescence microscopes. **(b)** Knockdown efficiency of TRIB3 mRNA expression measured by qRT-PCR. **(c)** Knockdown efficiency of TRIB3 protein expression measured by western blot. **(d)** TRIB3 knockdown suppressed ALP activity in hASCs in OM at 7 and 14 days. **(e)** TRIB3 knockdown inhibited mineralisation in hASCs in OM at 14 and 21 days. **(f)** TRIB3 knockdown downregulated mRNA expression of RUNX2, ALP, OSX and OCN in hASCs in OM at 7 and 14 days. $^{*}P < 0.05$.

Gene Ontology (GO) and pathway analyses. GO enrichment analyses, including biological processes (BP), cellular components (CC) and molecular functions (MF), were conducted using DAVID online software. For GO analyses, $P < 0.05$ was considered significant, and the results were shown as log10 (P value). Additionally, we identified the enriched networks and pathways in the IPA platform via a license from Ingenuity Systems.

Statistical analyses

Data were analysed using SPSS 25.0 software (IBM, Armonk, NY, USA). Comparisons between two groups were analysed using independent two-tailed Student t tests and comparisons between more than two groups were analysed using a one-way analysis of variance (ANOVA) followed by a Tukey post hoc test. The final results were expressed as mean ± standard deviation (SD). For all tests, the level of statistical significance was set at $P < 0.05$.

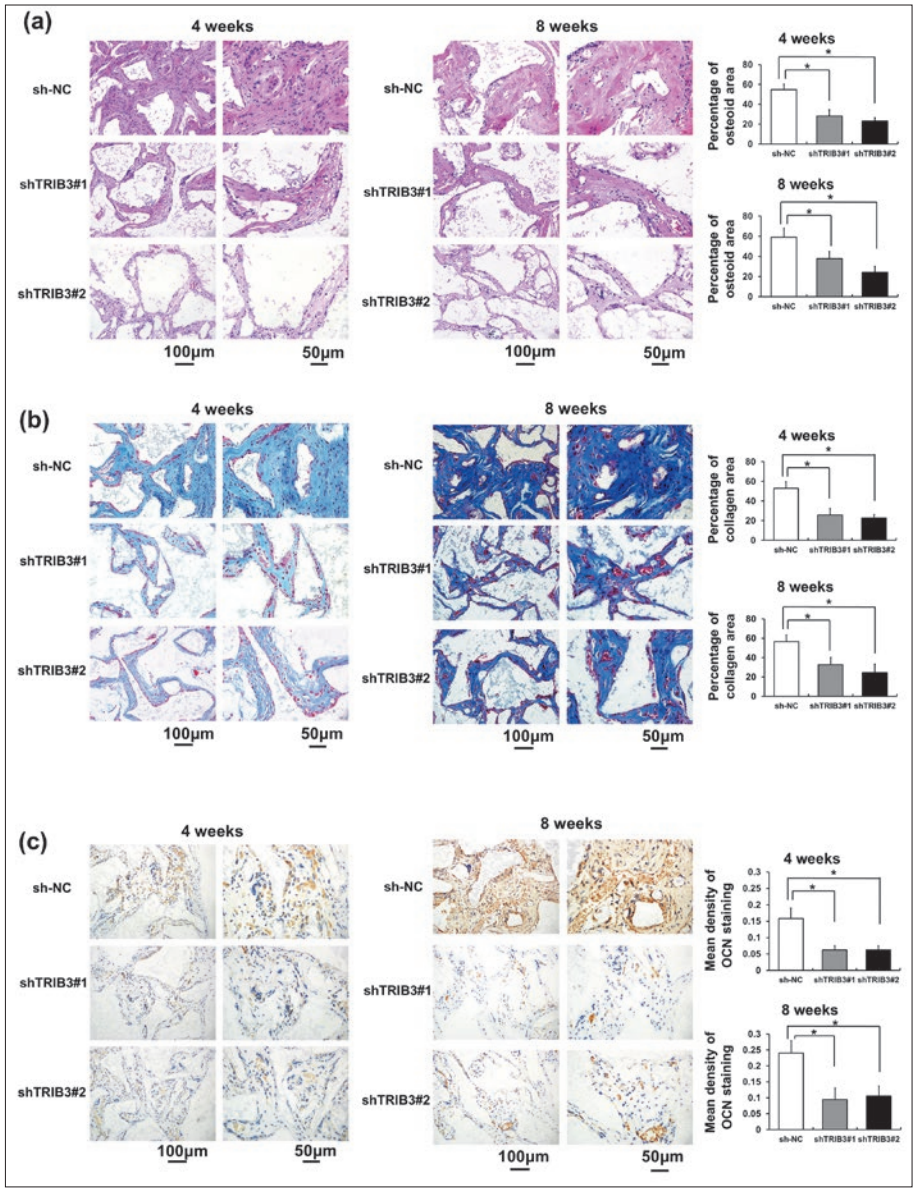

Fig 2 TRIB3 knockdown inhibited the osteogenic differentiation of hASCs in vivo. **(a)** H&E staining and osteoid quantification of sh-NC, shTRIB3#1 and shTRIB3#2 groups after 4 and 8 weeks of implantation. **(b)** Masson's trichrome staining and collagen quantification after 4 and 8 weeks of implantation. **(c)** Immunohistochemical staining and OCN-positive staining quantification after 4 and 8 weeks of implantation. $^{*}P < 0.05$.

Results

Knockdown of TRIB3 inhibited the osteogenic differentiation of hASCs in vitro

To explore the role of TRIB3 in the osteogenic differentiation of hASCs, we established stable TRIB3-knockdown hASCs using lentivirus-expressing TRIB3 shRNA. To avoid an off-target effect, two independent TRIB3 shRNA fragments were designed (Table S1, not published, provided on request). The knockdown efficiency of shTRIB3#1 and shTRIB3#2 was around 72% and 85%, respectively, as determined by fluorescence, qRT-PCR and western blot (Figs 1a to c). After osteoinduction for 7 and 14 days, the ALP activity decreased noticeably in TRIB3-knockdown hASCs, as observed by ALP staining (Fig 1d). ARS staining after osteoinduction for 14 and 21 days showed that extracellular matrix mineralisation was suppressed in TRIB3-knockdown hASCs (Fig 1e). The knockdown efficiency of shTRIB3#2 was better than shTRIB3#1, therefore mRNA expression of osteogenic genes, including RUNX2, OSX ALP and OCN, in shTRIB3#2 and sh-NC hASCs was examined after osteoinduction for 7 and 14 days. qRT-PCR results revealed that TRIB3 knockdown significantly inhibited the expression of RUNX2, OSX, ALP and OCN (Fig 1f). These results suggested that TRIB3 knockdown inhibited the osteogenic differentiation of hASCs in vitro.

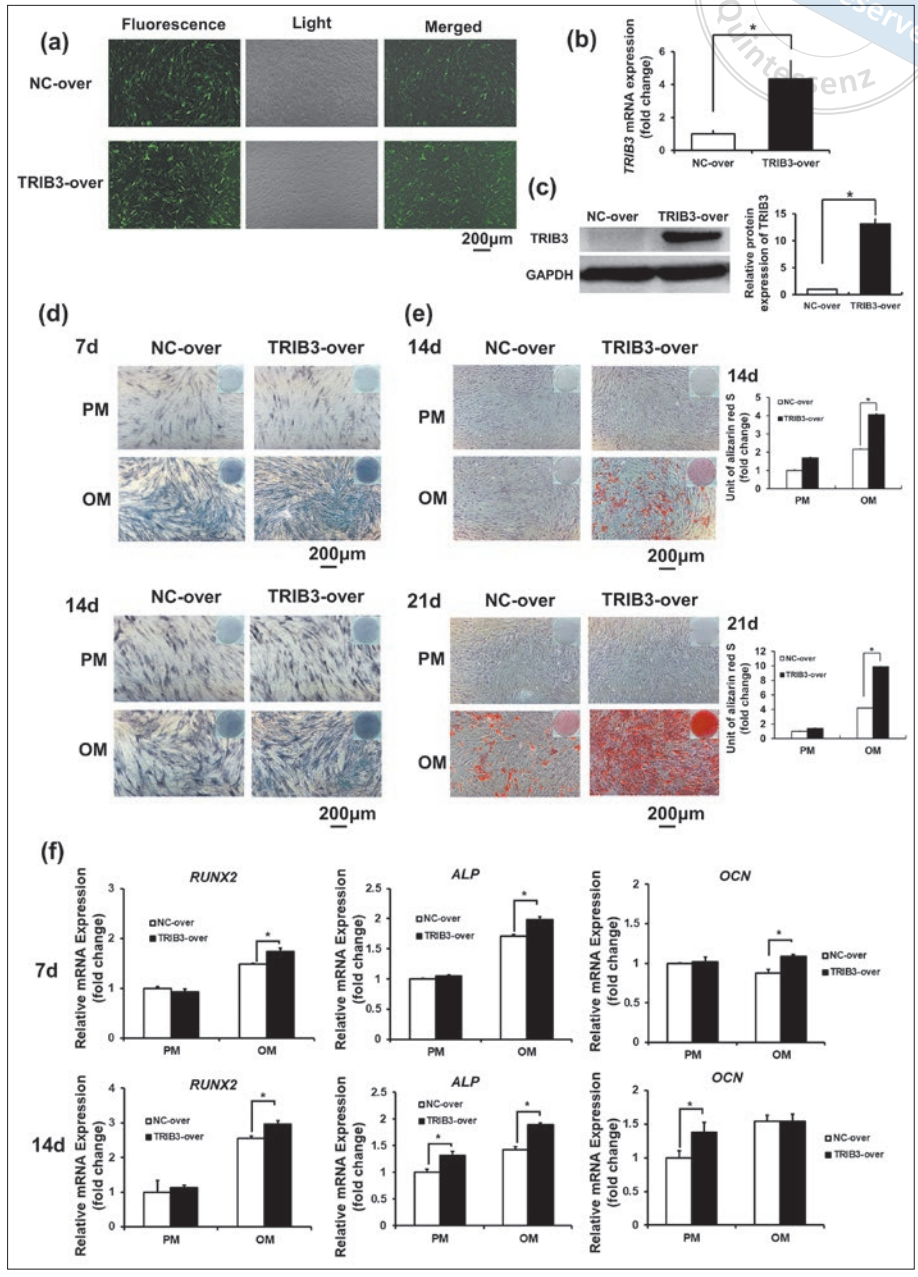

Fig 3 Overexpression of TRIB3 promoted the osteogenic differentiation of hASCs in vitro. **(a)** Microscopic images of GFP-positive hASCs after lentivirus (NC-over and TRIB3-over) transfection under light and fluorescence microscopes. **(b)** Overexpression efficiency of TRIB3 mRNA expression measured by qRT-PCR. **(c)** Overexpression efficiency of TRIB3 protein expression measured by western blot. **(d)** Overexpression of TRIB3 increased the ALP activity in hASCs in OM at 7 and 14 days. **(e)** Overexpression of TRIB3 upregulated mineralisation in hASCs in OM at 14 and 21 days. **(f)** Overexpression of TRIB3 upregulated mRNA expression of RUNX2, ALP and OCN in hASCs in OM at 7 and 14 days. $^{*}P < 0.05$.

TRIB3 knockdown inhibited the osteogenic differentiation of hASCs in vivo

TRIB3-knockdown-hASC-loaded β-TCP complexes were implanted into the dorsal subcutaneous spaces of nude mice (six mice per group at each time point). Transplants were harvested and subjected to histological analysis 4 and 8 weeks after surgery. H&E staining revealed obvious osteoid formation in the sh-NC group after 4 weeks of implantation (Fig 2a), while little osteoid could be observed in both shTRIB3#1 and shTRIB3#2 groups. After 8 weeks of implantation, there was more acidophilic neobone formation with fewer cells in the sh-NC group, but little osteoid could be observed in shTRIB3#1 and shTRIB3#2 groups (Fig 2a). Meanwhile, blue-stained collagen in Masson's trichrome staining was significantly higher in the sh-NC group compared with TRIB3 knockdown (shTRIB3#1 and shTRIB3#2) groups (Fig 2b). Furthermore, immunohistochemical staining for OCN indicated a larger range and higher intensity of positive-stained granules in the newly formed osteoid in the sh-NC group, especially after 8 weeks of implantation (Fig 2c).

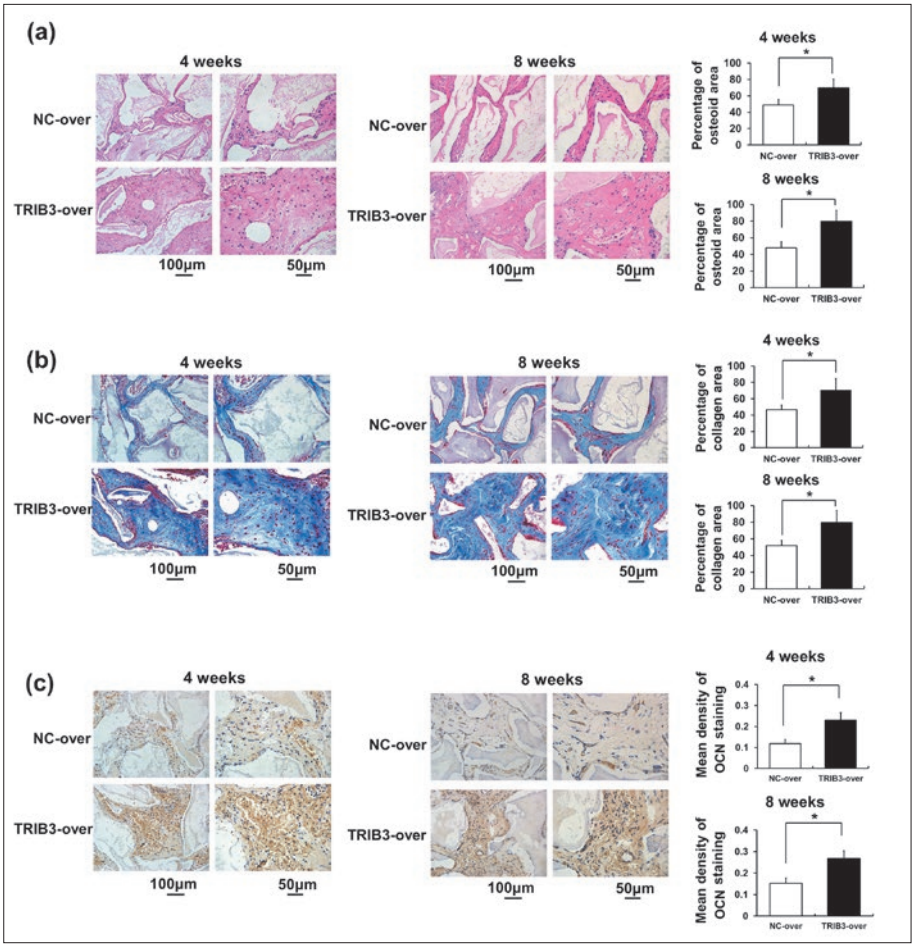

Fig 4 Overexpression of TRIB3 promoted the osteogenic differentiation of hASCs in vivo. **(a)** H&E staining and osteoid quantification of TRIB3-over and NC-over groups after 4 and 8 weeks of implantation. **(b)** Masson's trichrome staining and collagen quantification after 4 and 8 weeks of implantation. **(c)** Immunohistochemical staining and OC-positive staining quantification after 4 and 8 weeks of implantation. $^{*}P < 0.05$.

Overexpression of TRIB3 promoted osteogenic differentiation of hASCs in vitro

hASCs overexpressing TRIB3 (TRIB3-over) and its corresponding control group NC-over hASCs were established by lentivirus infection. The overexpression efficiency of TRIB3-over hASCs was more than four times greater than with NC-over hASCs, as determined by fluorescence observance, qRT-PCR and western blot (Figs 3a to c). After osteoinduction for 7 and 14 days, the ALP activity of hASCs increased noticeably in TRIB3-over hASCs, as determined from ALP staining (Fig 3d). ARS and quantification after osteoinduction for 14 and 21 days showed that extracellular matrix mineralisation was promoted significantly in TRIB3-over hASCs (Fig 3e). qRT-PCR results revealed that TRIB3 overexpression promoted the expression of osteogenic genes, including RUNX2 and ALP after osteoinduction at both days 7 and 14 (Fig 3f). OCN was upregulated at day 7 after osteoinduction, whereas at day 14 there was a significant increase in OCN mRNA expression without osteoinduction (Fig 3f). These results suggested that overexpression of TRIB3 promoted the osteogenic differentiation of hASCs in vitro.

Overexpression of TRIB3 promoted the osteogenic differentiation of hASCs in vivo

TRIB3-over hASCs and NC-over hASCs were incubated with β-TCP respectively and implanted into the dorsal subcutaneous spaces of nude mice. Transplants were also harvested at 4 and 8 weeks after surgery. H&E staining showed obvious acidophilic neobone formation in the TRIB3-over group compared with NC-over group even at 4 weeks after implantation (Fig 4a). Meanwhile, a large amount of blue-stained collagen was observed in the TRIB3-over group by Masson's trichrome staining at both 4 and 8 weeks after implantation (Fig 4b). Moreover, immunohistochemical staining for OCN showed more positive-stained granules in the newly formed bone tissue in the TRIB3-over group compared with the NC-over group after 4 and 8 weeks of implantation (Fig 4c).

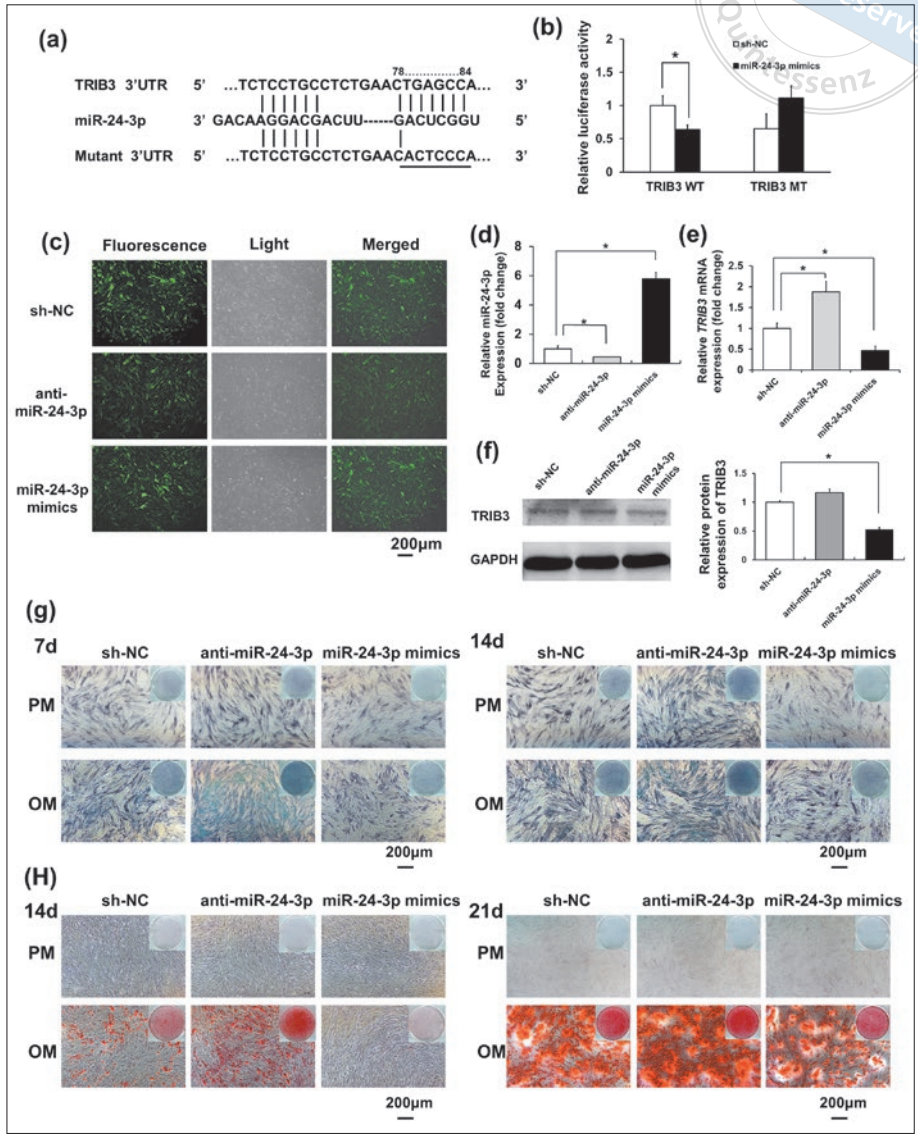

Fig 5 miR-24-3p inhibited TRIB3 expression and downregulated the osteogenic differentiation ability of hASCs. **(a)** The miR-24-3p potential target sites in TRIB3 transcripts predicted by RNA22 software. **(b)** Luciferase assay of miR-24-3p binding directly to TRIB3. **(c)** Microscopic images of GFP-positive hASCs after lentivirus (sh-NC, anti-miR-24-3p and miR-24-3p mimics) transfection under light and fluorescence microscopes. **(d)** Overexpression and knockdown efficiency of miR-24-3p measured by qRT-PCR. **(e)** Knockdown of miR-24-3p increased TRIB3 mRNA expression, and overexpression of miR-24-3p decreased TRIB3 mRNA expression. **(f)** Overexpression of miR-24-3p decreased TRIB3 protein expression, whereas knockdown of miR-24-3p did not influence TRIB3 protein expression significantly. **(g)** Knockdown of miR-24-3p upregulated ALP activity, whereas overexpression of miR-24-3p inhibited ALP activity in hASCs. **(h)** Knockdown of miR-24-3p upregulated mineralisation, whereas overexpression of miR-24-3p inhibited mineralisation in hASCs. $^{*}P < 0.05$.

miR-24-3p inhibited TRIB3 by targeting its 3'UTR and downregulated the osteogenic differentiation ability of hASCs

To further investigate the upstream regulating mechanism of TRIB3 expression, potential microRNAs targeting TRIB3 were predicted by miRbase, miRanda and RNA22, and finally miR-24-3p was selected according to preliminary experiments. The putative binding site of miR-24-3p in TRIB3 transcripts was predicted by RNA22 software (Thomas Jefferson University, Philadelphia, PA, USA) (Fig 5a). Dual-luciferase reporter assay showed that miR-24-3p suppressed the luciferase expression of vectors containing the 3'UTR of wild type TRIB3 (TRIB3-WT), but had no significant effect on the mutant-type TRIB3 (TRIB3-MT) (Fig 5b). To further investigate the effect of miR-24-3p on TRIB3 expression in hASCs, miR-24-3p knockdown (anti-miR-24-3p) and overexpression (miR-24-3p mimics) hASCs were established by lentivirus infection. The knockdown efficiency of anti-miR-24-3p was around 50% compared with sh-NC, as determined by fluorescence observance and qRT-PCR (Figs 5c and d). The overexpression efficiency of miR-24-3p mimics was approximately five times greater compared to sh-NC (Figs 5c and d). TRIB3 mRNA expression increased significantly in anti-miR-24-3p hASCs but decreased in miR-24-3p mimics hASCs (Fig 5e), whereas TRIB3 protein expression decreased in miR-24-3p mimics hASCs but did not change significantly in anti-miR-24-3p hASCs, as shown in western blot (Fig 5f).

Furthermore, the role of miR-24-3p in the osteogenic differentiation of hASCs was examined. After osteoinduction for 7 and 14 days, the ALP activity increased in anti-miR-24-3p hASCs but decreased in miR-24-3p-mimics hASCs, as observed by ALP staining (Fig 5g). ARS staining after 14 and 21 days of osteoinduction showed that extracellular matrix mineralisation was promoted in the anti-miR-24-3p group and suppressed in the miR-24-3p mimics group (Fig 5h). Thus, miR-24-3p inhibited TRIB3 by targeting its 3'UTR and downregulated the osteogenic differentiation ability of hASCs.

Bioinformatic analyses of the downstream signalling of TRIB3-mediated osteogenic differentiation of hASCs

To investigate the downstream signalling and molecular mechanisms of TRIB3-mediated osteogenic differentiation, total RNA of TRIB3-over and NC-over hASCs in PM or OM after 7 days were harvested. RNA sequencing and bioinformatic analyses were conducted. RNA sequencing data were deposited in RSA under the access code PRJNA633723. There were 148 DEGs when comparing TRIB3-over PM and NC-over PM (Table S2, not published, provided on request), and 245 when comparing TRIB3-over OM and NC-over OM (Table S3, not published, provided on request; Fig 6a). The expression level, log2FC and Q value of all DEGs are shown in Tables S2 to 5 (not published, provided on request), and the expression levels of representative DEGs are shown in the heatmap (Fig 6b). GO analysis revealed that TRIB3 was mainly involved in the processes of calcium ion binding and cell metabolism (Figs 6c and d). Very low-density lipoprotein receptor (VLDLR) and glutamate ionotropic receptor NMDA type subunit 1 (GRIN1) were downregulated (Figs 6b and e). On the other hand, protocadherin beta 12 (PCDHB12), an important factor related to calcium binding, was upregulated in TRIB3-over hASCs. Protocadherin beta 7 (PCDHB7) was upregulated in TRIB3-over hASCs, especially under osteoinductive conditions (Fig 6b).

IPA network analysis between TRIB3-over PM and NC-over PM revealed that ERK1/2 played an essential role in the process (Fig 7a), and analysis between TRIB3-over OM and NC-over OM revealed that the NF-κB signalling pathway was at the centre of the regulatory network (Fig 7b).

Discussion

In the present study, we revealed the important function of TRIB3 during the osteogenic differentiation of hASCs. TRIB3 promoted the osteogenic differentiation of hASCs both in vitro and in vivo. Moreover, miR-24-3p was identified as an inhibiting molecule of TRIB3 in hASCs and balanced the expression level of TRIB3 by post-transcriptional regulation. Furthermore, RNA sequencing and bioinformatic analyses showed that calcium ion binding, cellular metabolism, ERK1/2 and NF-κB pathways were likely to play crucial roles in the downstream regulations of TRIB3 in hASCs.

hASCs are capable of multilineage differentiation. Metabolic homeostasis controls the balance between osteoblast and adipocyte formation, and adipogenesis and osteogenesis have been considered to have an antagonistic relationship[5]. In our previous study, we found that TRIB3 inhibited the adipogenic differentiation of hASCs by inhibiting PPARγ expression[35]. Meanwhile, it was reported that TRIB3 blocked the adipogenesis of 3T3-L1 preadipocytes by disrupting the C/EBPβ transcriptional activity[36]. On the other hand, in the present study we revealed that TRIB3 promoted the osteogenic differentiation of hASCs, verifying the antagonism between osteogenic and adipogenic differentiation in hASCs. This result was consistent with the findings in human bone marrow-derived mesenchymal stem cells (hBMMSCs)[37]. Moreover, in this study we found that TRIB3 promoted the osteogenic differentiation of hASCs during the whole process of osteogenesis, as observed by qRT-PCR via early osteogenic marker RUNX2 mRNA expression, middle-stage markers OSX and ALP mRNA expression and ALP activity, and finally late-stage markers of mineralisation assay in vitro and OCN protein expression by immunohistochemical staining after 4 and 8 weeks of in vivo experiments. Furthermore, a small molecular drug, phenamil, was reported to work synergistically with BMP2 to promote osteogenic differentiation via stimulation of BMP signalling, and this combined medication could also enhance the expression of TRIB3 to facilitate osteogenesis for bone repair[38,39]. These findings would benefit the clinical transformation of TRIB3-mediated osteogenic differentiation of hASCs in bone tissue engineering by using small molecular drugs, a more convenient and safer method to enhance TRIB3 expression[32], but further efforts should be made regarding the efficiency and specificity of the candidate drugs or new investigations into more specified small molecular drugs to enhance TRIB3 expression in hASCs for future clinical application.

Although TRIB3 promotes the osteogenic differentiation of hASCs as revealed in this research both in vitro and in vivo, it also exerts multiple metabolic effects on other cells or tissues. Each important regulatory

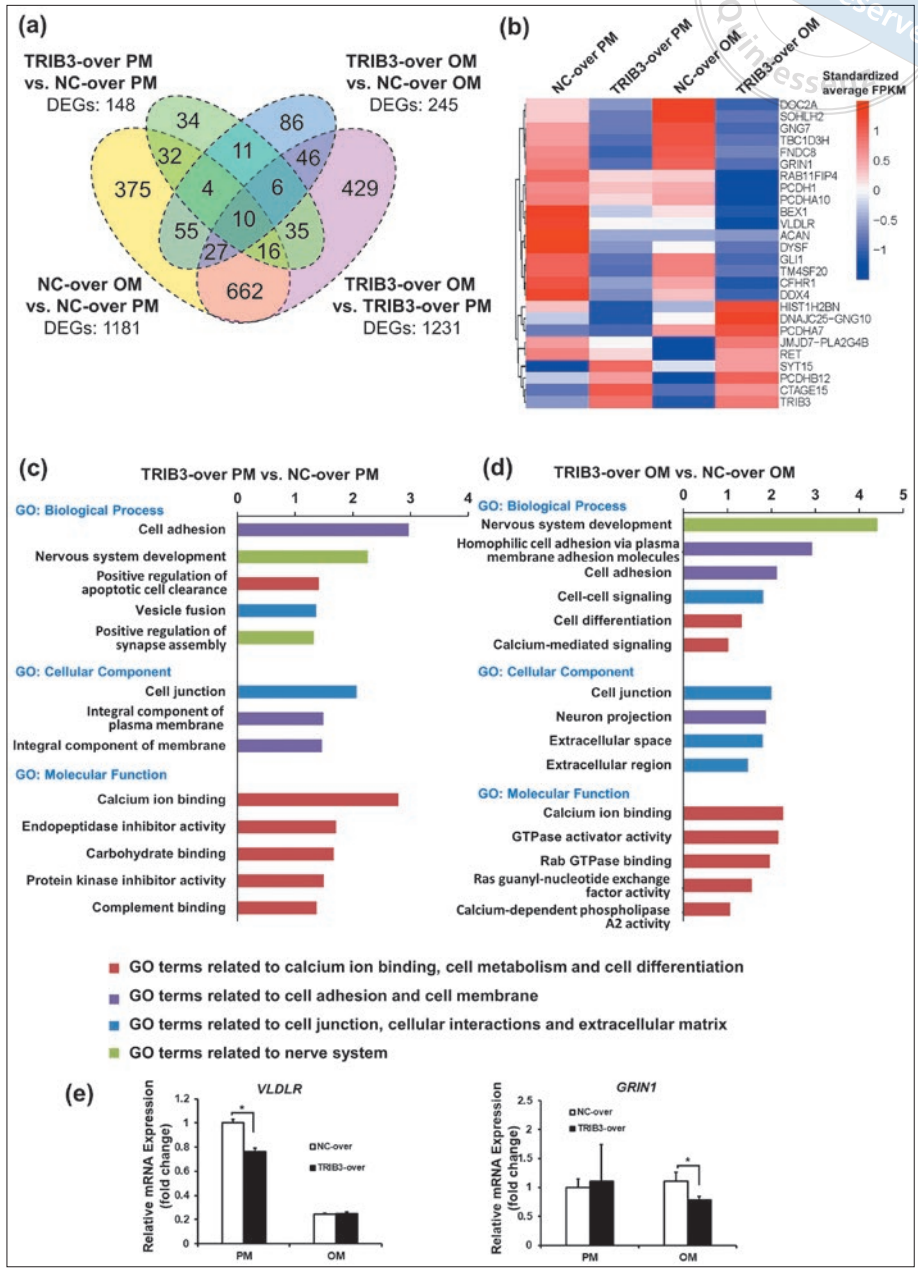

Fig 6 Bioinformatic analyses of TRIB3-overexpressing hASCs. **(a)** Distribution of DEGs comparing TRIB3-over PM and NC-over PM, TRIB3-over OM and NC-over OM, NC-over OM and NC-over PM, TRIB3-over OM and TRIB3-over PM. **(b)** Expression heatmap of representative DEGs. **(c)** GO analysis between TRIB3-over PM and NC-over PM. **(d)** GO analysis between TRIB3-over OM and NC-over OM. **(e)** Validation of representative DEGs. *$P < 0.05$.

factor commonly proves to be a double-edged sword[6]; thus, the controllability and balance of TRIB3 regulation is paramount to its further applications. Excessive expression of TRIB3 may lead to metabolic disorders. For example, TRIB3 inhibited insulin signalling by binding directly to Akt, thus blocking Akt activation in the liver[9]. Meanwhile, TRIB3 interacted with the transcription factor ATF4 to form the complex that acts as a competitive inhibitor of cAMP response element-binding (CREB) transcription factor in the regulation of key exocytosis genes in pancreatic β cells[40]. TRIB3 missense Q84R polymorphism, gain-of-function polymorphism of TRIB3 with the R84 variant, led to insulin resistance and endothelial dysfunction with increased risk of type II diabetes and cardiovascular diseases[41-43]. It is therefore essential to gain further insight into the upstream regulation molecules that could balance the expression of TRIB3 and the downstream regulatory network of TRIB3.

Epigenetic regulation, including DNA methylation, histone modification and RNA interference, has been found to play important roles in the regulation of stem cell fate. For example, various regulatory enzymes of histone modification, such as histone H3K4 demethy-

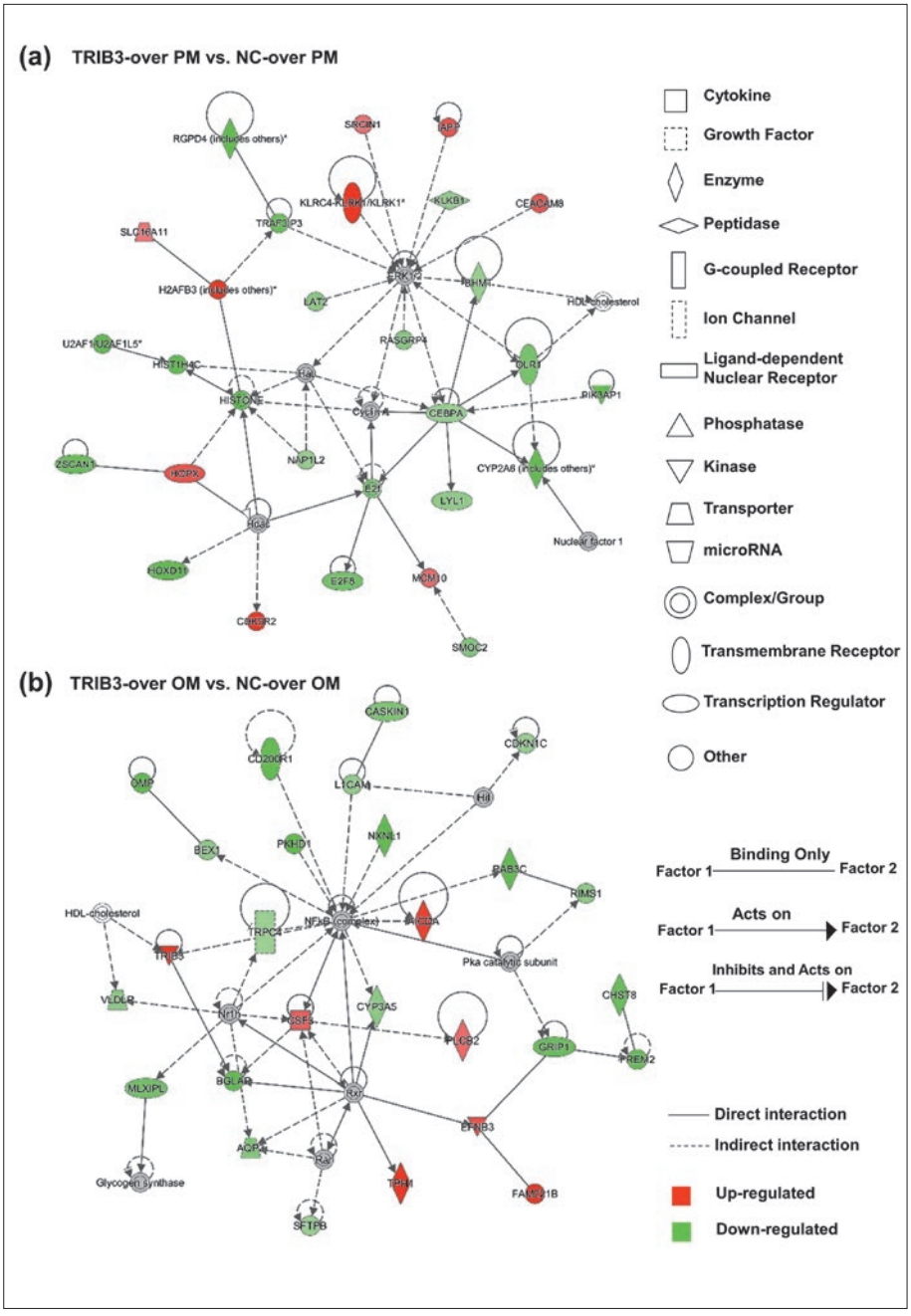

Fig 7 Network analyses of TRIB3-overexpressing hASCs. **(a)** Between TRIB3-over PM and NC-over PM. **(b)** Between TRIB3-over OM and NC-over OM.

lase RBP2[28,44] and LSD1[32,45], H3K9 acetyltransferase PCAF[46] and histone deacetylases HDAC2[47], have been reported to regulate the osteogenic differentiation of mesenchymal stem cells. Meanwhile, the microRNA network comprises one of the most important forms of epigenetic regulation. By binding partially or fully complementary with the 3'UTR of targeted mRNAs, microRNAs negatively regulate the mRNA or protein expression of the targeted genes through post-transcriptional regulation. In previous studies, we reported that several microRNAs, such as miR-34a[48], miR-137[49], miR-140-5p[50], miR-375[34,51] and miR-3648[52], could target different molecules or signalling pathways to regulate the osteogenic differentiation of mesenchymal stem cells, thus revealing the important regulatory functions of the microRNA network[30]. Thus, in the present study, we predicted the potential microRNAs that could target TRIB3 using miRbase, miRanda and RNA22 software. After comprehensive analyses of microRNA sequences, complementary conditions of binding sites and binding energy with the 3'UTR of TRIB3, we finally focused on miR-24-3p after preliminary experiments. Based

on dual luciferase reporter assay, we proved that miR-24-3p could directly bind to the predicted binding sites on the 3'UTR of TRIB3 and inhibited the expression of TRIB3. Meanwhile, miR-24-3p was reported to be highly expressed in the trabecular bone of osteoporotic patients[53,54], indicating that miR-24-3p might be a negative regulator of osteogenesis. In this study, we confirmed the role of miR-24-3p in the osteogenic differentiation of hASCs and that miR-24-3p indeed inhibited the osteogenesis of hASCs by inhibiting TRIB3. Therefore, the expression of TRIB3 could be levelled by miR-24-3p, which permitted regulatory controllability and promoted osteogenesis through an important metabolic target while obtaining a safe and controllable effect via post-transcriptional epigenetic regulation.

With regard to the downstream regulatory network of TRIB3, we utilised RNA sequencing and bioinformatic analyses to obtain an overall map of gene expressions after TRIB3-overexpression in hASCs. According to GO analyses, TRIB3 played an important role in calcium ion binding and cellular metabolism. Calcium ions (Ca^{2+}) have been regarded as important endogenous divalent ions that regulate bone hemostasis mainly through the calcium signalling pathways[55-58]. In this research, we found that calcium binding–related genes, including protocadherin α7 (PCDHA7), protocadherin β12 (PCDHB12) andsynaptotagmin 15 (SYT15), were upregulated after TRIB3 overexpression, while very low density lipoprotein receptor (VLDLR), glutamate ionotropic receptor NMDA type subunit 1 (GRIN1) and aggrecan (ACAN) were downregulated. Meanwhile, it has been reported that ERK1/2 and NF-κB pathways are closely related to calcium regulation[59], which is in accordance with the IPA pathway analyses in this research. When comparing TRIB3-over PM and NC-over PM, ERK1/2 was at the regulatory centre of important differentiated genes, and the activation of ERK1/2 was recognised to promote the osteogenic differentiation of mesenchymal stem cells[37]. When comparing TRIB3-over OM and NC-over OM, NF-κB played an important role at the core of the regulatory network, and the inhibition of NF-κB and inflammatory response was considered to promote osteogenesis[60].

Collectively, TRIB3 promoted the osteogenic differentiation of hASCs levelled by miR-24-3p through post-transcriptional epigenetic regulation. For the downstream regulatory network, TRIB3 regulated calcium ion binding, cellular metabolism and the ERK1/2 and NF-κB pathways to promote osteogenic differentiation hASCs; however, further studies on the validation and specific roles of other differentially-expressed genes and the regulatory mechanisms through the ERK1/2 and NF-κB pathways are required.

Conclusion

TRIB3 is a promising therapeutic target for hASC-based bone tissue engineering, and the epigenetic regulation of TRIB3 through miR-24-3p permits regulatory controllability, thus promoting osteogenesis through an important metabolic target while obtaining a safe and controllable effect via post-transcriptional epigenetic regulation.

Conflicts of interest

The authors declare no conflicts of interest related to this study.

Author contribution

Dr Xiang Song BAI performed the experiments, collection and/or assembly of data, data analysis and interpretation and manuscript writing; Drs Ping ZHANG, Yun Song LIU and Hao LIU performed the experiments, collection and/or assembly of data, data analysis and interpretation; Dr Long Wei LV conceived and designed the research and performed the experiments, collection and/or assembly of data, data analysis and interpretation and manuscript writing. financial support; Prof Yong Sheng ZHOU conceived and designed the research, provided administrative support and revised the manuscript.

(Received Dec 18, 2020; accepted May 10, 2021)

References

1. Grayson WL, Bunnell BA, Martin E, Frazier T, Hung BP, Gimble JM. Stromal cells and stem cells in clinical bone regeneration. Nat Rev Endocrinol 2015;11:140–150.
2. Barba M, Di Taranto G, Lattanzi W. Adipose-derived stem cell therapies for bone regeneration. Expert Opin Biol Ther 2017;17:677–689.
3. Tewary M, Shakiba N, Zandstra PW. Stem cell bioengineering: Building from stem cell biology. Nat Rev Genet 2018;19:595–614.
4. Rando TA, Ambrosio F. Regenerative rehabilitation: Applied biophysics meets stem cell therapeutics. Cell Stem Cell 2018;22:306–309.
5. Rauch A, Haakonsson AK, Madsen JGS, et al. Osteogenesis depends on commissioning of a network of stem cell transcription factors that act as repressors of adipogenesis. Nat Genet 2019;51:716–727.
6. Richmond L, Keeshan K. Pseudokinases: A tribble-edged sword. FEBS J 2020;287:4170–4182.
7. Eyers PA, Keeshan K, Kannan N. Tribbles in the 21st century: The evolving roles of tribbles pseudokinases in biology and disease. Trends Cell Biol 2017;27:284–298.

8. Mondal D, Mathur A, Chandra PK. Tripping on TRIB3 at the junction of health, metabolic dysfunction and cancer. Biochimie 2016;124: 34–52.
9. Du K, Herzig S, Kulkarni RN, Montminy M. TRB3: A tribbles homolog that inhibits Akt/PKB activation by insulin in liver. Science 2003;300:1574–1577.
10. Szabat M, Page MM, Panzhinskiy E, et al. Reduced insulin production relieves endoplasmic reticulum stress and induces β cell proliferation. Cell Metab 2016;23:179–193.
11. Zhang W, Liu J, Tian L, Liu Q, Fu Y, Garvey WT. TRIB3 mediates glucose-induced insulin resistance via a mechanism that requires the hexosamine biosynthetic pathway. Diabetes 2013;62:4192–4200.
12. Okamoto H, Latres E, Liu R, et al. Genetic deletion of Trb3, the mammalian Drosophila tribbles homolog, displays normal hepatic insulin signaling and glucose homeostasis. Diabetes 2007;56:1350–1356.
13. Kwon M, Eom J, Kim D, et al. Skeletal muscle tissue Trib3 links obesity with insulin resistance by autophagic degradation of AKT2. Cell Physiol Biochem 2018;48:1543–1555.
14. Wang ZH, Shang YY, Zhang S, et al. Silence of TRIB3 suppresses atherosclerosis and stabilizes plaques in diabetic ApoE-/-/LDL receptor-/- mice. Diabetes 2012;61:463–473.
15. Li K, Zhang TT, Hua F, Hu ZW. Metformin reduces TRIB3 expression and restores autophagy flux: An alternative antitumor action. Autophagy 2018;14:1278–1279.
16. Prudente S, Sesti G, Pandolfi A, Andreozzi F, Consoli A, Trischitta V. The mammalian tribbles homolog TRIB3, glucose homeostasis, and cardiovascular diseases. Endocr Rev 2012;33:526–546.
17. Sowers JR. Role of TRIB3 in diabetic and overnutrition-induced atherosclerosis. Diabetes 2012;61:265–266.
18. Lorenzi M, Altmann A, Gutman B, et al. Alzheimer's disease neuroimaging initiative. Susceptibility of brain atrophy to TRIB3 in Alzheimer's disease, evidence from functional prioritization in imaging genetics. Proc Natl Acad Sci U S A 2018;115:3162–3167.
19. Ambrosi TH, Scialdone A, Graja A, et al. Adipocyte accumulation in the bone marrow during obesity and aging impairs stem cell-based hematopoietic and bone regeneration. Cell Stem Cell 2017;20: 771–784.e6.
20. Treiber T, Treiber N, Meister G. Regulation of microRNA biogenesis and its crosstalk with other cellular pathways. Nat Rev Mol Cell Biol 2019;20:5–20.
21. Kozomara A, Birgaoanu M, Griffiths-Jones S. miRBase: From microRNA sequences to function. Nucleic Acids Res 2019;47(D1):D155–D162.
22. Gebert LFR, MacRae IJ. Regulation of microRNA function in animals. Nat Rev Mol Cell Biol 2019;20:21–37.
23. Grigelioniene G, Suzuki HI, Taylan F, et al. Gain-of-function mutation of microRNA-140 in human skeletal dysplasia. Nat Med 2019;25:583–590.
24. Lian JB, Stein GS, van Wijnen AJ, et al. MicroRNA control of bone formation and homeostasis. Nat Rev Endocrinol 2012;8:212–227.
25. Chang CC, Venø MT, Chen L, et al. Global microRNA profiling in human bone marrow skeletal-stromal or mesenchymal-stem cells identified candidates for bone regeneration. Mol Ther 2018;26: 593–605.
26. Rupaimoole R, Slack FJ. MicroRNA therapeutics: Towards a new era for the management of cancer and other diseases. Nat Rev Drug Discov 2017;16:203–222.
27. Kristensen LS, Andersen MS, Stagsted LVW, Ebbesen KK, Hansen TB, Kjems J. The biogenesis, biology and characterization of circular RNAs. Nat Rev Genet 2019;20:675–691.
28. Lv L, Liu Y, Zhang P, et al. The nanoscale geometry of TiO2 nanotubes influences the osteogenic differentiation of human adipose-derived stem cells by modulating H3K4 trimethylation. Biomaterials 2015;39:193–205.
29. Li Z, Liu X, Zhu Y, et al. Mitochondrial phosphoenolpyruvate carboxykinase regulates osteogenic differentiation by modulating AMPK/ULK1-dependent autophagy. Stem Cells 2019;37: 1542–1555.
30. Lv L, Liu Y, Zhang P, et al. The epigenetic mechanisms of nanotopography-guided osteogenic differentiation of mesenchymal stem cells via high-throughput transcriptome sequencing. Int J Nanomedicine 2018;13:5605–5623.
31. Zhu Y, Zhang X, Gu R, et al. LAMA2 regulates the fate commitment of mesenchymal stem cells via hedgehog signaling. Stem Cell Res Ther 2020;11:135.
32. Lv L, Ge W, Liu Y, et al. Lysine-specific demethylase 1 inhibitor rescues the osteogenic ability of mesenchymal stem cells under osteoporotic conditions by modulating H3K4 methylation. Bone Res 2016;4:16037.
33. Tang Y, Lv L, Li W, et al. Protein deubiquitinase USP7 is required for osteogenic differentiation of human adipose-derived stem cells. Stem Cell Res Ther 2017;8:186.
34. Chen S, Zheng Y, Zhang S, Jia L, Zhou Y. Promotion effects of miR-375 on the osteogenic differentiation of human adipose-derived mesenchymal stem cells. Stem Cell Reports 2017;8:773–786.
35. Bai XS, Lv LW, Zhou YS. Tribbles pseudokinase 3 inhibits the adipogenic differentiation of human adipose-derived mesenchymal stem cells [in Chinese]. Beijing Da Xue Xue Bao Yi Xue Ban 2020;52:1–9.
36. Bezy O, Vernochet C, Gesta S, Farmer SR, Kahn CR. TRB3 blocks adipocyte differentiation through the inhibition of C/EBPbeta transcriptional activity. Mol Cell Biol 2007;27:6818–6831.
37. Zhang C, Hong FF, Wang CC, et al. TRIB3 inhibits proliferation and promotes osteogenesis in hBMSCs by regulating the ERK1/2 signaling pathway. Sci Rep 2017;7:10342.
38. Fan J, Im CS, Cui ZK, et al. Delivery of phenamil enhances BMP-2-induced osteogenic differentiation of adipose-derived stem cells and bone formation in calvarial defects. Tissue Eng Part A 2015;21: 2053–2065.
39. Fan J, Pi-Anfruns J, Guo M, et al. Small molecule-mediated tribbles homolog 3 promotes bone formation induced by bone morphogenetic protein-2. Sci Rep 2017;7:7518.
40. Liew CW, Bochenski J, Kawamori D, et al. The pseudokinase tribbles homolog 3 interacts with ATF4 to negatively regulate insulin exocytosis in human and mouse beta cells. J Clin Invest 2010;120: 2876–2888.
41. Qin RR, Song M, Li YH, et al. Association of increased serum Sema3E with TRIB3 Q84R polymorphism and carotid atherosclerosis in metabolic syndrome. Ann Clin Lab Sci 2017;47:47–51.
42. Fischer Z, Das R, Shipman A, et al. A *Drosophila* model of insulin resistance associated with the human TRIB3 Q/R polymorphism. Dis Model Mech 2017;10:1453–1464.
43. Prudente S, Bailetti D, Mendonca C, et al. Infrequent TRIB3 coding variants and coronary artery disease in type 2 diabetes. Atherosclerosis 2015;242:334–339.
44. Ge W, Shi L, Zhou Y, et al. Inhibition of osteogenic differentiation of human adipose-derived stromal cells by retinoblastoma binding protein 2 repression of RUNX2-activated transcription. Stem Cells 2011;29:1112–1125.
45. Ge W, Liu Y, Chen T, et al. The epigenetic promotion of osteogenic differentiation of human adipose-derived stem cells by the genetic and chemical blockade of histone demethylase LSD1. Biomaterials 2014;35:6015–6025.
46. Zhang P, Liu Y, Jin C, et al. Histone H3K9 acetyltransferase PCAF is essential for osteogenic differentiation through bone morphogenetic protein signaling and may be involved in osteoporosis. Stem Cells 2016;34:2332–2341.
47. La Noce M, Mele L, Laino L, et al. Cytoplasmic interactions between the glucocorticoid receptor and HDAC2 regulate osteocalcin expression in VPA-treated MSCs. Cells 2019;8:217.

48. Fan C, Jia L, Zheng Y, et al. MiR-34a promotes osteogenic differentiation of human adipose-derived stem cells via the RBP2/NOTCH1/CYCLIN D1 coregulatory network. Stem Cell Reports 2016;7:236–248.
49. Ma X, Fan C, Wang Y, et al. MiR-137 knockdown promotes the osteogenic differentiation of human adipose-derived stem cells via the LSD1/BMP2/SMAD4 signaling network. J Cell Physiol 2020;235:909–919.
50. Li Z, Jin C, Chen S, et al. Long non-coding RNA MEG3 inhibits adipogenesis and promotes osteogenesis of human adipose-derived mesenchymal stem cells via miR-140-5p. Mol Cell Biochem 2017;433:51–60.
51. Chen S, Tang Y, Liu Y, et al. Exosomes derived from miR-375-overexpressing human adipose mesenchymal stem cells promote bone regeneration. Cell Prolif 2019;52:e12669.
52. Min Z, Xiaomeng L, Zheng L, et al. Asymmetrical methyltransferase PRMT3 regulates human mesenchymal stem cell osteogenesis via miR-3648. Cell Death Dis 2019;10:581.
53. Seeliger C, Karpinski K, Haug AT, et al. Five freely circulating miRNAs and bone tissue miRNAs are associated with osteoporotic fractures. J Bone Miner Res 2014;29:1718–1728.
54. Kelch S, Balmayor ER, Seeliger C, Vester H, Kirschke JS, van Griensven M. miRNAs in bone tissue correlate to bone mineral density and circulating miRNAs are gender independent in osteoporotic patients. Sci Rep 2017;7:15861.
55. Sundelacruz S, Moody AT, Levin M, Kaplan DL. Membrane potential depolarization alters calcium flux and phosphate signaling during osteogenic differentiation of human mesenchymal stem cells. Bioelectricity 2019;1:56–66.
56. Ballard A, Zeng R, Zarei A, et al. The tethering function of mitofusin2 controls osteoclast differentiation by modulating the Ca^{2+}-NFATc1 axis. J Biol Chem 2020;295:6629–6640.
57. Wang S, Li S, Hu M, Huo B. Calcium response in bone cells at different osteogenic stages under unidirectional or oscillatory flow. Biomicrofluidics 2019;13:064117.
58. Pei S, Parthasarathy S, Parajuli A, et al. Perlecan/Hspg2 deficiency impairs bone's calcium signaling and associated transcriptome in response to mechanical loading. Bone 2020;131:115078.
59. Zeng H, Pathak JL, Shi Y, et al. Indirect selective laser sintering-printed microporous biphasic calcium phosphate scaffold promotes endogenous bone regeneration via activation of ERK1/2 signaling. Biofabrication 2020;12:025032.
60. Jimi E, Aoki K, Saito H, et al. Selective inhibition of NF-kappa B blocks osteoclastogenesis and prevents inflammatory bone destruction in vivo. Nat Med 2004;10:617–624.